JOURNAL OF CATALYSIS **164,** 131–145 (1996)
ARTICLE NO. 0369

Hydrothermal Stability of Cerium Modified Cu-ZSM-5 Catalyst for Nitric Oxide Decomposition

Yanping Zhang[1] and Maria Flytzani-Stephanopoulos*,[2]

*Department of Chemical Engineering, Massachusetts Institute of Technology, Cambridge, Massachusetts 02139; and *Department of Chemical Engineering, Tufts University, Medford, Massachusetts 02155*

Received July 28, 1995; revised June 17, 1996; accepted June 18, 1996

Effects of cerium(III) ions are reported in this paper on the activity and hydrothermal stability of Cu-ZSM-5 catalysts for nitric oxide decomposition in water vapor-containing gas streams. Wet conditions drastically decrease the NO decomposition activity of unpromoted Cu-ZSM-5 catalysts at 500°C. Activity is partially recovered upon removal of water vapor. Copper ion species migration leading to CuO formation inside the zeolite channels has been identified by STEM/EDX, XRD, and XPS as the major pathway to deactivation. The cerium modified Cu-ZSM-5 displays higher wet-gas activity for NO decomposition and recovers a higher fraction of its initial dry-gas activity than the Cu-ZSM-5 catalyst after removal of water vapor. The presence of cerium suppresses CuO particle formation and dealumination, providing higher hydrothermal stability for the zeolite structure and higher copper dispersion, all of which contribute to better catalytic performance of the Ce,Cu-ZSM-5 materials.

INTRODUCTION

The direct catalytic decomposition of nitric oxide is the most attractive way for removing NO_x from flue gas streams since it involves no reductant addition, such as ammonia or hydrocarbons. The most promising catalyst for NO decomposition is presently the copper ion-exchanged ZSM-5 zeolite, first reported by Iwamoto *et al.* (1, 2) to have stable activity even in the presence of oxygen. Several studies of this catalyst system have been reported in the literature in recent years (3–11). Typically, a maximum in the NO conversion to N_2 at 500°C is reported for Cu-ZSM-5 (1–3). The high-temperature (>450°C) activity of Cu-ZSM-5 is enhanced by addition of co-cations (12, 13). This is more pronounced in oxygen-containing gas streams (14).

All NO_x-containing combustion off-gases also contain a significant amount of water vapor (2–15%), hence the hydrothermal stability of the catalyst is of great importance for practical applications. However, a stable active catalyst resistant to water vapor still eludes the art. Iwamoto *et al.* (15) and Li and Hall (16) reported that the catalytic activity of Cu-ZSM-5 for NO decomposition was decreased in the presence of 2% water vapor, but could be recovered after removal of water vapor. Details about these tests were not given in the articles. However, Kharas and co-workers (17) found that Cu-ZSM-5 was quickly and severely deactivated in simulated lean-burn gas including 10% H_2O at $GHSV = 127{,}000\ h^{-1}$ at 600 and 800°C. The authors claimed that sintering of the catalytically active components, rather than degradation of the metastable zeolite support, probably dominated the deactivation.

Recent work in this laboratory (14) has shown that severe steaming (20% water at 600°C for 20 h) of Na-ZSM-5 zeolite leads to partial vitreous glass formation and dealumination, which results in loss of micropore volume and a much reduced Cu^{2+} cation uptake capacity. Under reaction conditions in the presence of water vapor (20% H_2O–1.6% NO–He balance, 500°C, 10–20 h), Cu-ZSM-5 catalysts suffered a drastic loss of activity. Under-exchanged Cu-ZSM-5 was inferior to excessively exchanged ($2\ Cu/Al \times 100\% > 100\%$) catalysts in terms of the wet gas activity and dry gas activity recovery. Alkaline earth, Y^{3+}, and Ce^{3+}-modified Cu-ZSM-5 catalysts were superior to the unpromoted catalysts in terms of dry gas activity recovery. Particularly interesting was the Ce,Cu-ZSM-5 catalyst which also retained wet NO decomposition activity twice as high as that of Cu-ZSM-5 at various water concentrations.

In this paper we report on detailed comparisons of Ce,Cu-ZSM-5 with Cu-ZSM-5 catalysts in wet NO gas mixtures. Fresh, steamed and used catalyst samples were examined by luminescence, powder X-ray diffraction (XRD), scanning transmission electron microscopy (STEM)/X-ray microprobe analysis, and X-ray photoelectron spectroscopy (XPS) to identify differences in the state and distribution of the copper and cerium cations in the zeolite samples. These structural differences are, in turn, used to explain measured reactivity differences.

[1] Current address: Air Products and Chemicals, Inc., 7201 Hamilton Blvd., Allentown, PA 18195.
[2] To whom correspondence should be addressed.

0021-9517/96 $18.00

EXPERIMENTAL

Catalysts. Table 1 shows the preparation and composition of the catalysts used in this study. Four types of catalysts, Cu^{2+} ion-exchanged, Ce^{3+} ion-exchanged, Ce^{3+} and Cu^{2+} ion-exchanged ZSM-5, and Ce^{3+} impregnated Cu^{2+} ion-exchanged ZSM-5, were prepared. Metal ion-exchanged zeolite catalysts, namely Cu-ZSM-5, Ce-ZSM-5, and Ce,Cu-ZSM-5 catalysts, were prepared by incorporating metal cations into a Na-ZSM-5 zeolite (Si/Al = 21.5, SMR 6-2670-1191, Davison Chemical Division, W. R. Grace & Co.), while the Ce-impregnated material, Ce/Cu-ZSM-5, was prepared by impregnating with cerium nitrate the copper ion-exchanged ZSM-5. The Cu-ZSM-5 catalyst was prepared by copper ion exchange in an aqueous 0.007*M* cupric acetate solution at room temperature for 19 h. The initial pH of the aqueous cupric acetate solution was 5.74, while the final pH was 5.65. The Cu-exchange process was carried out once for low Cu ion exchange, and thrice for high Cu exchange level. After the exchanges, the sample was filtered, and washed with deionized water twice at room temperature for 45 minutes; then it was dried in air at 100°C overnight. The Ce-ZSM-5 was prepared by exchange of Ce^{3+} cations with the Na-ZSM-5 in a dilute (0.007*M*) aqueous cerium nitrate solution at 85°C for 2 h. After Ce-exchange, the Ce-ZSM-5 sample was filtered and washed with deionized water at room temperature, dried in air at 100°C for 10 h, then calcined in air at 500°C for 2 h. Three Ce-ZSM-5 catalysts were prepared by this procedure (see Table 1). The Ce,Cu-ZSM-5 catalyst was prepared by sequential exchange of Ce^{3+} and Cu^{2+} cations with the Na-ZSM-5 zeolite. First, cerium was exchanged. The resulting Ce,Na-ZSM-5 material was then exchanged with copper ions following the procedure described above.

The Ce-impregnated catalyst, Ce/Cu-ZSM-5, was prepared as follows: After cerium nitrate was dissolved in deionized water, a certain amount of Cu(136)-ZSM-5 was added to the cerium nitrate solution corresponding to an atomic ratio of Ce/Al = 0.2. This atomic ratio gave the same total amount of cerium as in the Ce(60),Cu(136)-ZSM-5 (ion-exchanged material). The slurry was left at 25°C for 5 days, then dried at 100°C for 10 h. The material was finally calcined in air at 500°C for 2 h.

Elemental analyses were performed by inductively coupled plasma emission spectrometry (ICP, Perkin–Elmer Plasma 40) after the catalyst samples were dissolved in special solutions purchased from UniSolv, Inc., for measuring Ce concentration. HF solutions could not be prepared because Ce^{3+} species are fluoride insoluble. The reagents consisted of three types of solutions: UA-4, UNS-2A and UNS-2B. The UA-4, containing HF, dissolves the catalyst, the UNS-2A and UNS-2B neutralize and stabilize the solution to (i) deactivate the HF by increasing the pH to a value of 7.5 to 8.0 and (ii) maintain solubility of the samples. The copper exchange levels were 72 and 141% in the two Cu-ZSM-5 materials, respectively. The cerium exchange levels for the three Ce-ZSM-5 materials were 11, 26, and 60%. The Ce and Cu exchange levels were 60% and 138%, respectively, in the Ce,Cu-ZSM-5. The Cu or Ce exchange level is defined as 2 Cu/Al × 100% or 3 Ce/Al × 100%, respectively, where the metal ratios are measured by ICP. Table 1 shows the atomic ratios of Na, Cu, Ce to Al after the exchange steps of the catalysts examined in this work.

TABLE 1

Summary of Catalyst Preparation[a]

Catalysts	Si/Al	Cu/Al[b]	Ce/Al[b]	Na/Al	Ce,Cu exch. times
Na-ZSM-5[c]	21.5			1.0	
Cu-ZSM-5	19.9	0.36 (72%)		0.25	0, 1
Cu-ZSM-5	20.3	0.705 (141%)		~0	0, 3
Ce-ZSM-5	20.4		0.034 (11%)	0.72	1, 0
Ce-ZSM-5	20.7		0.088 (26%)	0.58	2, 0
Ce-ZSM-5	20.8		0.20 (60%)	0.52	3, 0
Ce,Cu-ZSM-5	19.5	0.69 (138%)	0.20 (60%)	~0	3, 3
Ce,Cu-ZSM-5		0.59 (119%)	0.037 (11%)		1, 2
Ce,Cu-ZSM-5	19.6	0.675 (135%)	0.13 (40%)		3, 3
Ce/Cu-ZSM-5[d]	20.0	0.68 (136%)	0.2	~0	3/-

[a] Each exchange of Ce was performed in 0.007*M* $Ce(NO_3)_3$ aqueous solution at 85°C for 2 h, while each Cu exchange was at RT for 19 h in 0.007*M* $Cu(ac)_2$ aqueous solution.

[b] The values in parentheses are ion exchange levels based on Al and cation contents as measured by ICP, and assuming a valence of +2 for Cu and +3 for Ce.

[c] As-received Na-ZSM-5: SMR-2670-1191 (Davison).

[d] Ce was impregnated on Cu(136)-ZSM-5 from $Ce(NO_3)_3$ aq. solution in a slurry with Ce/Al = 0.2; left at 25°C for 5 days, then dried at 100°C for 10 h. The material was finally calcined in air at 500°C for 2 h.

Reaction studies. The NO decomposition activity of the catalysts was evaluated in a laboratory-scale (1.1 cm I.D.), quartz reactor system (13). An amount of 0.5 g of catalyst in fine powder form (<5 μm) was placed in the reactor for NO conversion measurements. The reactor pressure was about 1.4 atm. The contact time, W/F, defined as the ratio of catalyst weight in the reactor to total flowrate of the feed gas stream, was 1.0 g s/cm^3 (corresponding GHSV = 1,800 h^{-1}, NTP). Pure He (Airco, 99.999%) flowing through deionized water in a constant temperature water saturator was used to feed water vapor to the reactor through an electrically heated line. A Matheson certified standard gas mixture of

4% NO–He was mixed with the pure He to a desired inlet gas mixture composition.

The fresh catalysts were pretreated in pure He in the reactor at 500°C for 2 h before they were exposed to the reactant stream. The catalyst activity was evaluated in both dry and wet gas mixtures. All measurements were made after the reaction had reached steady-state. A dry-ice cold trap was installed at the reactor exit to condense the water vapor prior to analyzing the exhaust gas in a gas chromatograph (HP: Model 5890) equipped with a thermal conductivity detector. A 5A molecular sieve column of 1/8 in. O.D. by 6 ft. long, was used to separate N_2, O_2, and NO in the effluent stream. Based on the reaction stoichiometry, the NO conversion to N_2 is calculated as ($2 \times N_2$ concentration in the effluent flow)/(NO concentration in the feed stream) $\times$ 100%. The gas chromatograph also monitored overall conversion of NO. However, this is not accurate and was not used in this work. The reason is that gas phase reaction of the unreacted NO with product oxygen to form NO_2 takes place at the cooler exhaust gas line (13, 16). In regard to the formation of N_2O as a by-product, this has been shown to be negligible above ~400°C on Cu-ZSM-5 (16).

Characterization of catalyst samples. Cerium(III) luminescence spectra were recorded on a SPEX spectrofluorometer (Model No. 1501 and 1502) equipped with DM 3000 Software, SPEX Industries. The spectra of fresh and used Ce-ZSM-5 and Ce,Cu-ZSM-5 materials were recorded by loading about 0.3 g of the material into a quartz cell.

A VG HB603 scanning transmission electron microscope was used to characterize the fresh and steamed catalyst samples. The catalyst samples were supported on a 200 mesh, carbon film-coated, plain nickel grid in the STEM chamber. Prior to this preparation, the samples were calcined in a muffle furnace in air at 500°C for 2 h. Coating by carbon in vacuum was used to ensure no particle charging during the STEM analysis. The bulk composition of the catalyst samples was analyzed by energy dispersive X-ray (EDX) microprobe technique (spot size: 0.5 nm by 1 nm), and Cu, Ce, Si, and Al distributions were simultaneously collected by an X-ray mapping technique with a magnification of 1×10^6.

A Rigaku 300 X-ray powder diffractometer was used to examine the crystal structures of the fresh and steamed catalysts, as well as to check for CuO particle formation. The samples were evacuated at 55°C for 24 h, then placed in a dessicator. The diffraction patterns were taken in the 2θ range of 5–80° at a scanning speed of 1°/min.

A Perkin–Elmer Model 548 XPS (ESCA) instrument with 2 mm spatial resolution was used to determine the elemental concentrations of copper, cerium, oxygen, and silicon on the surface of the catalyst samples. A Mg$K\alpha$ anode X-ray source (300 W, 15 KV) providing high signal intensity and 178 eV of a fixed pass energy was used. The base pressure in the vacuum chamber was lower than 7.5×10^{-8} Torr (1 Torr = 133.3 Pa). A layer of catalyst sample in powder form was pressed on a double-sided transfer tape adhered on a 1″ by 0.5″ aluminum sheet. The sample was then introduced into the XPS vacuum chamber and placed on a sample holder. Total time for acquisition of the Cu, Ce, O, and Si core level spectra was 20 min after the sample had been exposed to the X-ray beam for 10 min. Atomic ratios of copper, cerium, and oxygen to silicon in the surface region of the catalyst crystal were determined based on these spectra.

Effect of steaming on cation exchange sites of ZSM-5. Understanding the catalyst deactivation due to steaming is important for application of these catalysts. However, it is difficult quantitatively to distinguish between copper-induced and dealumination-induced catalyst deactivation by using XRD and STEM analyses. The loss of ion exchange capacity of steamed or used catalysts was measured in this work to indicate the extent of dealumination. These tests were conducted as follows: The used catalysts were removed from the reactor, and treated with a solution of 0.05*M* HNO_3 for 4 h to dissolve all the exchanged copper. This procedure does not affect the framework aluminum. The catalysts were then washed with deionized water, exchanged with Na^+ using 0.01*M* $NaNO_3$ solution for 10 h, dried in air at 100°C for 10 h, and heated at 500°C for 2 h. A small amount of the catalyst samples was analyzed by ICP to determine the residual amount of copper. The nitric acid would not dissolve any copper oxide associated with extra-lattice aluminum oxide (copper aluminate). The remaining material was ion-exchanged with copper acetate solution thrice, following the procedures described earlier. The catalysts were filtered and dried overnight in air at 100°C, and the amount of re-exchanged copper ion was measured by ICP. Subsequently, the NO conversion to N_2 over the re-exchanged catalysts was measured. The analyses of the catalysts and the conditions of steaming are given in Table 2.

RESULTS

Evaluation of Catalyst Activity

Dry NO-decomposition. The NO conversion to N_2 over the Ce(11)-, Ce(26)-, and Ce(60)-ZSM-5, Cu(141)-ZSM-5, Ce(11),Cu(119)-, and Ce(60),Cu(138)-ZSM-5 catalysts was evaluated in a gas mixture of 2% NO–He, at a contact time of 1.0 g s/cm^3 (NTP) over the temperature range of 350–600°C, as shown in Fig. 1. We have recently reported (13) that Mg^{2+} modified Cu-ZSM-5 showed significantly higher NO conversion to N_2 than Cu-ZSM-5 in the high-temperature region (450–600°C), while a low Ce^{3+}-containing Cu-ZSM-5 promoted the catalyst activity in the low temperature region (300–450°C). Figure 1 shows that the conversion of NO to N_2 over the Ce(60),Cu(138)-ZSM-5 is higher than that over Cu(141)-ZSM-5 in the low-temperature region (350–450°C), while Ce(11),Cu(119)-ZSM-5 was even more active in this region. All Ce-ZSM-5 materials had very low activity for NO decomposition. The

TABLE 2

Effects of Cations on Hydrothermal Stability/Activity of Ion-Exchanged Cu-ZSM-5

Catalysts	Si/Al	Cu/Al	Cu/Al
(cation-ZSM-5)		(remaining Cu)	(removed Cu)
Cu(141)-[a]	20.3	0.17	0.54
Cu(141)-[b]	22.8	0.30	0.41
Cu(141)-[c]	20.2	0.13	0.58
Cu(141)-[d]	21.1	0.07	0.64
Ce(40)/Cu(135)-[a]	21.5	0.19	0.49
Ce(40)/Cu(135)-[b]	22.8	0.32	0.36
Ce(60)-[b, e]	22.0	—	—
Catalysts	Si/Al	Cu/Al	Cu/Al(re-exchanged)
Cu(141)-[a]	20.4	0.65	0.47
Cu(141)-[b]	22.9	0.57	0.27
Cu(141)-[c]	20.3	0.68	0.56
Cu(141)-[d]	21.3	0.78	0.71
Ce(40)/Cu(135)-[a]	21.0	0.77	0.60
Ce(40)/Cu(135)-[b]	22.9	0.67	0.35
Ce(60)-[b, e]	22.1	—	0.41
Na-ZSM-5[a]	20.5	0.67	0.67
Na-ZSM-5[f]	22.1		0.10

Note. The upper portion of the table shows samples that after steaming were washed with 0.05*M* HNO_3 for 4 h, then with 0.01*M* $NaNO_3$ for 10 h. The samples were then dried at 100°C for 10 h and calcined at 500°C for 2 h. The lower portion of the table gives ICP measurements after the samples in the upper portion were ion-exchanged with 0.007*M* $Cu(ac)_2$ at room temperature for 20 h thrice.

[a] At 500°C; catalytically steamed in 20% H_2O–2% NO−He for 10 h, then in 2% NO + He for 20 h.

[b] At 600°C; catalytically steamed in 20% H_2O–2% NO−He for 10 h, then in 2% NO–He for 20 h.

[c] At 500°C steamed in 20% H_2O–4% O_2–He for 10 h and reacted in 2% NO–He for 20 h.

[d] Reacted in 2% NO + He for 20 h at 500°C.

[e] Steamed and dried at 600°C.

[f] At 600°C steamed in 20% H_2O–2% O_2–He for 10 h, then in 2% NO–He for 20 h.

Ce(60),Cu(138)-ZSM-5 also showed higher catalytic activity than the Cu(141)-ZSM-5 in the 5% O_2-containing gas stream, as shown in Fig. 2. This is also true for the Mg,Cu-ZSM-5 catalysts in 5% O_2-gas mixture (13, 14).

The oxygen-free, dry gas-conversion of NO to N_2, 92% and 91%, respectively, for Cu(141)-ZSM-5 and Ce(60), Cu(138)-ZSM-5 at 500°C is used as the basis to calculate relative NO conversion to N_2 in wet gas conditions.

Wet NO-decomposition. A series of tests were performed at 500°C in 2% NO−He at contact time of 1.0 g s/cm^3 (NTP), under both dry (0% H_2O) and wet (2–20% H_2O) conditions over the Cu-ZSM-5, Ce,Cu-ZSM-5, and impregnated Ce/Cu-ZSM-5 catalysts. Figure 3 shows the steady-state NO conversion to N_2 over the catalysts Cu(72)-, Cu(141)-, Ce(11),Cu(119)-, Ce(60),Cu(138)-ZSM-5, and impregnated Ce(60)/Cu(136)-ZSM-5 in dry (2% NO–He)

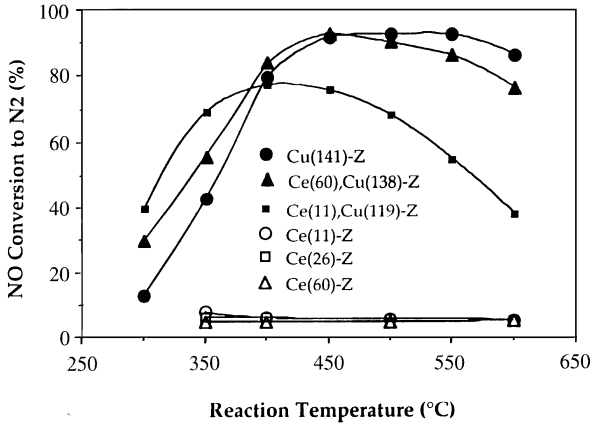

FIG. 1. NO conversion over Ce-ZSM-5, Cu-ZSM-5, and Ce modified Cu-ZSM-5 catalysts in 2% NO–He, at W/F = 1.0 g s/cm^3 (NTP).

and wet gas mixtures (20% H_2O–2% NO–He). After the catalysts were treated in pure He for 2 h and in 2% NO–He for 4 h, water vapor was introduced in the reactant gas mixture. The presence of water vapor drastically decreased the NO conversion. The wet-gas activities reached a steady state of 8–10% conversion of NO to N_2 for all the catalysts, except 20% conversion for Ce(60),Cu(138)-ZSM-5, in 2 h.

The activity recovery in dry NO–He gas after removal of water vapor from the gas stream is also shown in Fig. 3. For the excessively exchanged Cu(141)-ZSM-5, about 30% of the original dry gas conversion was recovered after removal of water vapor. However, no recovery was found for the Cu(72)-ZSM-5 catalyst. It is interesting that the impregnated Ce(60)/Cu(138)-ZSM-5 shows a similar performance to Cu(141)-ZSM-5 for NO decomposition. The Ce(11),Cu(119)-ZSM-5 gradually restored its activity to about 40% of the original value. The Ce(60),Cu(138)-ZSM-5 catalyst was again superior to Cu(141)-ZSM-5 and all other Ce,Cu-ZSM-5 catalysts

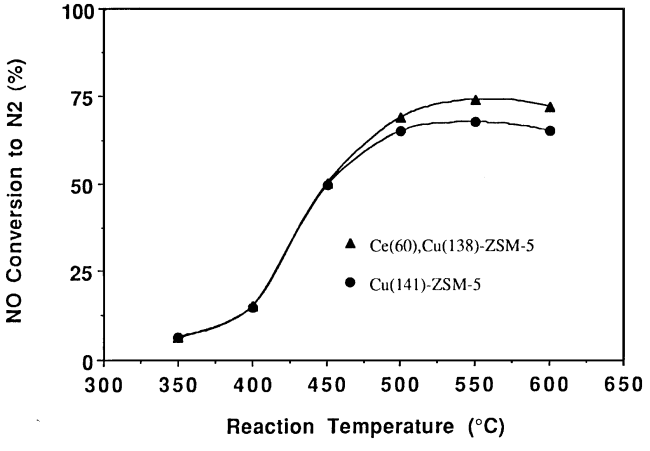

FIG. 2. NO conversion over Cu(141)-ZSM-5 and Ce(60),Cu(138)-ZSM-5 catalysts in 2% NO–5% O_2–He, at W/F = 1.0 g s/cm^3 (NTP).

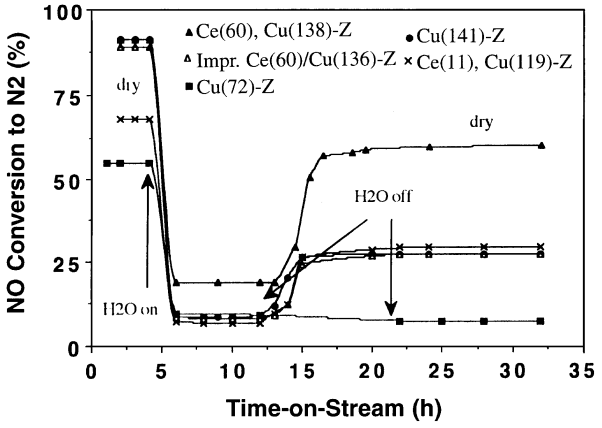

FIG. 3. Effect of H_2O vapor on the NO conversion to N_2 over Cu-ZSM-5 and various Ce-modified Cu-ZSM-5 catalysts in 20% H_2O–2% NO–He, at W/F = 1.0 g s/cm^3 (NTP) and 500°C.

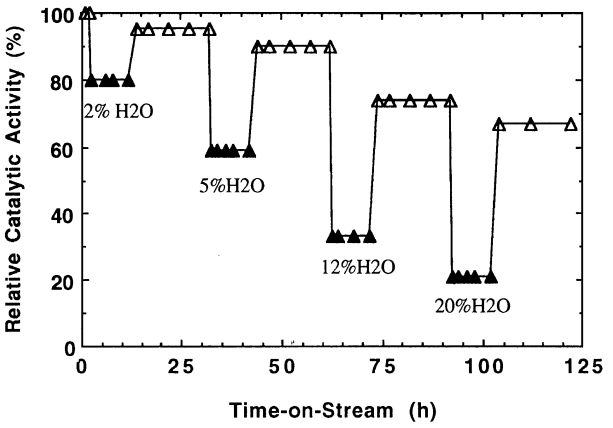

FIG. 5. Cyclic performance of Ce(60),Cu(138)-ZSM-5 in dry/wet NO decomposition in 2% NO–He, at W/F = 1.0 g s/cm^3 (NTP) and 500°C.

shown in Fig. 3 relative to dry gas-activity recovery (more than 67%). The Ce(60),Cu(138)-ZSM-5 catalyst was, thus, chosen for additional testing.

Activities of the catalysts Ce(60),Cu(138)-ZSM-5 and Cu(141)-ZSM-5 were measured in a 2% NO–He stream with varying water vapor contents from 2 to 20% at 500°C. Cyclic activity tests in dry and wet conditions were conducted. The results of dry/wet gas cycles for Cu(141)-ZSM-5 and Ce(60),Cu(138)-ZSM-5 are shown in Figs. 4 and 5, respectively, where the relative catalytic activity, defined as the ratio of steady-state activity to the initial dry-gas activity, is shown by the horizontal lines. The catalysts were pretreated in He at 500°C for 2 h prior to introduction of the reactant gas stream (2% NO–He). Following this dry-gas test for 2 h, the catalysts were exposed to 2% water vapor for 10 h followed by dry reaction for 20 h. Next, NO conversion to N_2 was measured in cycles of wet and dry reaction gases (with different water vapor contents). The transition time between wet/dry and dry/wet-gas conversion was about 2 h. The Cu(141)-ZSM-5 catalyst was inferior to Ce(60),Cu(138)-ZSM-5 at all conditions. The latter displays twice as high activity as the former in all wet gas mixtures. The dry-gas activities of the used samples were not affected by treating the samples in pure He at high temperatures (600–750°C).

Figure 6 shows the relative NO conversion to N_2 over the Cu(141)-ZSM-5 and Ce(6),Cu(138)-ZSM-5 in dry (2% NO–He) and wet gas (20% H_2O–2% NO–He) mixtures at 400°C. After removal of water vapor, the dry-gas activity of each catalyst was recovered much more than for the 500°C-steamed samples. Again, the Ce(60),Cu(138)-ZSM-5 restored a larger fraction of its original activity than the Cu(141)-ZSM-5 catalyst. Figure 6 also shows differences in the rate of activity recovery between the two catalysts.

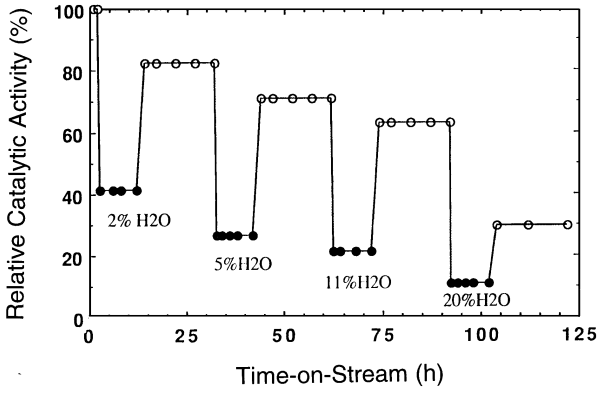

FIG. 4. Cyclic performance of Cu(141)-ZSM-5 in dry/wet NO decomposition in 2% NO–He, at W/F = 1.0 g s/cm^3 (NTP) and 500°C.

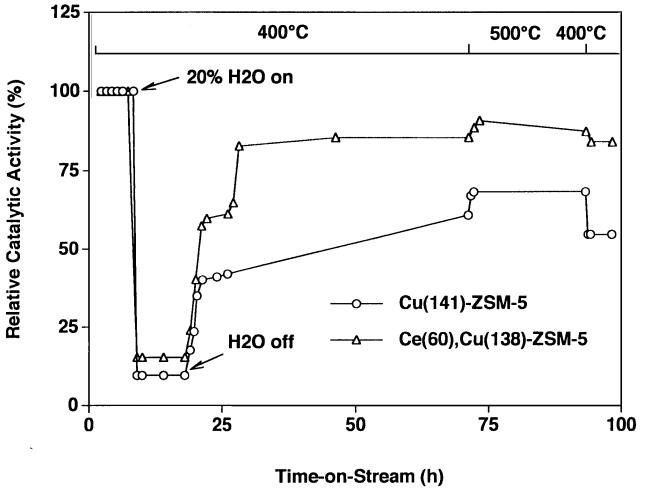

FIG. 6. Dry/wet NO conversion to N_2 over Cu(141)-ZSM-5 and Ce(60),Cu(138)-ZSM-5 in 20% H_2O–2% NO–He, at W/F = 1.0 g s/cm^3 (NTP) and 400°C.

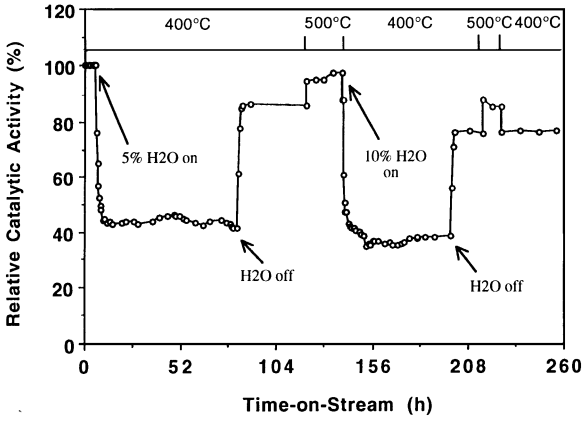

FIG. 7. NO conversion to N_2 over Cu(141)-ZSM-5 in 5% and 10% H_2O–2% NO–He at 400°C; and in 2% NO–He at 400 and 500°C, respectively, at W/F = 1.0 g s/cm^3 (NTP).

Figure 7 shows the relative NO conversion to N_2 over the Cu(141)-ZSM-5 catalyst in dry (2% NO–He) and wet gas (5% and 10% H_2O− 2% NO−He) mixtures at 1.0 g s/cm^3 (NTP) and 400°C. Upon introduction of 5% H_2O into the reaction stream, the relative catalytic activity rapidly decreased to 42% and remained constant in the wet gas for 77 h. The 500°C-dry gas activity was almost completely recovered after removal of water vapor from the reaction stream. After further steaming at 400°C in 10% H_2O-containing gas for 54 h, followed by removing the water vapor, the catalytic activity was restored to 85% of its initial dry gas-value at 500°C. However, the 400°C-dry gas activity recovery was lower than the 500°C-dry gas activity in both cases.

Catalyst Characterization

XRD, STEM/EDX, and XPS analyses were performed to examine physical and chemical changes of the fresh and catalytically used Cu(141)-ZSM-5 and Ce(60),Cu(138)-ZSM-5 samples. Luminescence was used to check for trivalent cerium ions in the cerium-exchanged zeolites. Fresh, 100°C-dried samples are referred to as as-synthesized. Air-calcined samples were prepared by calcining the as-synthesized samples in air at 500°C for 2 h. For the catalysts used in dry- and wet-gas streams, three treatments were examined: (1) in He for 2 h, then in 2% NO–He at 500°C for 4 h; (2) in 20% H_2O–2% NO–He at 500°C for 10 h following treatment-1; (3) in 2% NO−He at 500°C for 20 h following treatment-2.

Cerium(III) identification by luminescence. Fresh and catalytically used Ce(60),Cu(138)-ZSM-5 materials were examined by luminescence to identify whether Ce^{3+} had been ion-exchanged into ZSM-5. It was found that excitation light at wavelength of 295 nm maximized the Ce^{3+} photoluminescence intensity at 359 nm which is the characteristic line of the Ce^{3+} luminescence in Ce^{3+} ion-exchanged Y zeolites (18). The Ce^{3+} luminescence spectrum of the fresh Ce(60),Cu(138)-ZSM-5 is shown in Fig. 8 with a doublet at 346.4 and 358.3 nm. Assignments of Ce^{3+} transitions for the doublet are $^2D \rightarrow {}^2F_{5/2}$ for 346.4 nm and $^2D \rightarrow {}^2F_{7/2}$ by analogy to that of Ce^{3+} in zeolites X and Y (19). The Ce^{3+} luminescence spectrum of the used Ce(60),Cu(138)-ZSM-5, reacted in 2% NO–He over the temperature range of 350–600°C for 48 h, is similar to that of the fresh sample, except that the luminescence intensity is lower. This decrease in luminescence intensity is in agreement with the literature (18).

Characterization of samples by STEM. STEM/EDX mappings (scale of a mapping: 100 nm by 120 nm) of Al and Cu, for Cu(141)-ZSM-5 in the fresh, 500°C air-calcined state, and after 10-h wet- and 20-h dry-NO decomposition (under the conditions of Fig. 3), are shown in Fig. 9. Uniform Al and Cu distribution and strong Cu association with

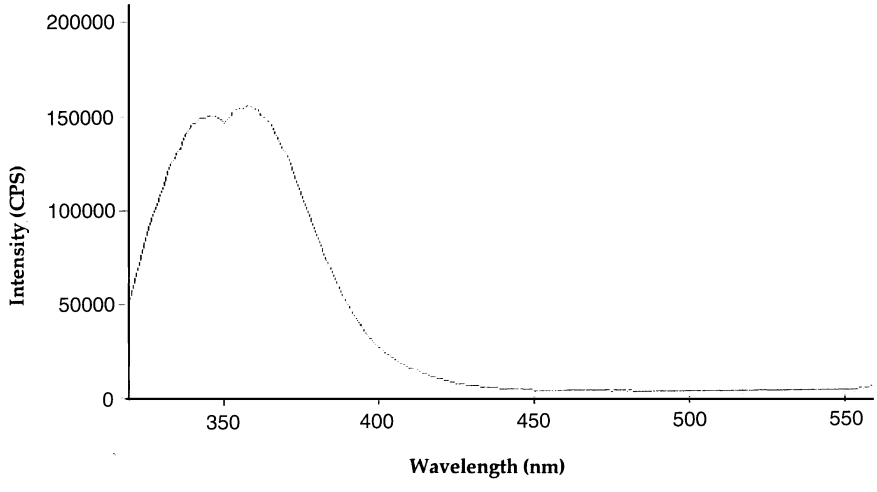

FIG. 8. Ce^{3+} luminescence of fresh Ce(60),Cu(138)-ZSM-5 at room temperature, $\lambda_{exc} = 295$ nm.

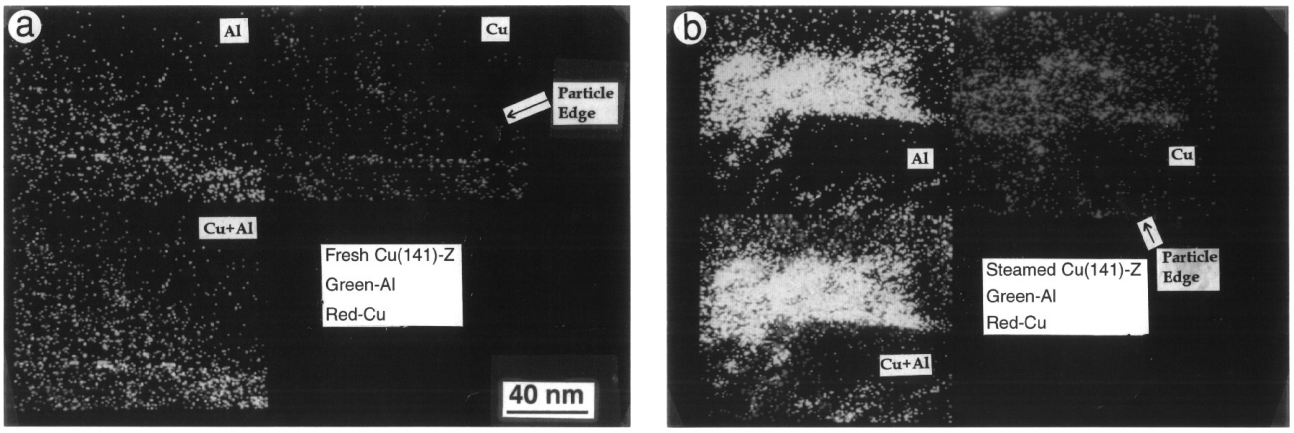

FIG. 9. STEM/X-ray mapping of Al and Cu in Cu(141)-ZSM-5. (a) 500°C-calcined fresh sample; (b) catalytically used sample in 20% H_2O–2% NO–He for 10 h, then in 2% NO–He at 500°C for 20 h (scale of a mapping: 100 nm by 120 nm).

Al in the air-calcined Cu(141)-ZSM-5 samples are found, as shown in Fig. 9a (the Al mapping is in the upper left corner, the Cu mapping is in the upper right corner, and the overlap of the Al and Cu mappings is in the lower left corner). The 500°C-steamed Cu(141)-ZSM-5 catalyst, however, shows many CuO particles, as can be seen in Fig. 9b, with mean aggregate sizes of about 15 nm as estimated from the electron micrographs. Interestingly, aluminum aggregates are also seen, which indicates partial dealumination of the zeolite.

Cerium and aluminum distributions were obtained for the 500°C-air calcined Ce(60)-ZSM-5 by using STEM/EDX. Cerium was well distributed in the ZSM-5 zeolite crystal, but it also enriched the crystal surface. It is plausible that cerium on the external surface of ZSM-5 is in oxidic form, while the uniformly distributed Ce ions are associated with framework aluminum. As shown in Table 1, the Na/Al ratio was reduced during the catalyst preparation, confirming ion exchange. This result is in good agreement with the Ce^{3+} luminescence data.

Three samples of Ce(60),Cu(138)-ZSM-5 were examined by STEM/EDX mapping: sample 1 is fresh, 500°C air-calcined material, sample 2 is reacted in the gas stream under treatment-2, and sample 3 is after treatment-3 (refer to Fig. 3). As shown in Fig. 10a, Cu, Al, and Ce are uniformly distributed in sample 1 except for one Ce/Cu aggregate on the right-hand side of the crystal. In sample 2, copper enrichment can be seen on the edges of the catalyst crystal (see Fig. 10b). Unlike the catalytically used Cu(141)-ZSM-5 shown in Fig. 9b, however, no Al aggregates were found in sample 2. After removal of water vapor from the reactant stream, the Cu and Ce cations are redistributed in the Ce(60),Cu(138)-ZSM-5 samples, as shown in Fig. 10c. The mapping for sample 3 is shown in Fig. 10c. From comparison of the copper distribution in sample 3 with that in the fresh Cu(141)-ZSM-5 and Ce(60),Cu(138)-ZSM-5, it was found that the redistributed Cu cannot reach the same uniform dispersion as in the fresh samples. The STEM picture of the 500°C-steamed Ce(60),Cu(138)-ZSM-5 shown in Fig. 10d depicts a few very fine (<3 nm in diameter) clusters. Therefore, 100% activity recovery cannot be achieved.

X-Ray diffraction patterns. XRD analyses of the fresh and used Cu(141)-ZSM-5 and Ce(60),Cu(138)-ZSM-5 catalysts after treatment-3 were performed to examine the Cu-containing phase and potential structural changes of the zeolitic structure. The XRD patterns of the fresh, 500°C-air calcined Cu(141)-ZSM-5 and Ce(60),Cu(138)-ZSM-5 samples are shown in Fig. 11 along with the parent Na-ZSM-5 in the range of $2\theta = 34$–$40°$ in which the CuO crystal has the strongest diffraction peak. No CuO phase is present in the fresh samples. However, Fig. 12 shows CuO particle formation for the 500°C-steamed Cu(141)-ZSM-5. Using the Scherrer formula, the CuO particles are about 20 nm in size. On the other hand, CuO formation is not evident from the XRD-pattern of the 500°C-steamed Ce(60),Cu(138)-ZSM-5 sample after treatment-3 (Fig. 12). No other crystalline phases involving copper or cerium were identified by XRD in these samples.

For the 400°C-steamed Cu(141)-ZSM-5 and Ce(60), Cu(138)-ZSM-5 samples, under the conditions of Figs. 6 and 7, no CuO diffraction peaks were observed on the XRD patterns.

XRD analysis of the fresh and used Cu(141)-ZSM-5 and Ce(60),Cu(138)-ZSM-5 after treatment-3 showed XRD pattern similar to the parent Na-ZSM-5, except for diffraction peak shift of the steamed samples. Figure 13a shows that the fresh Cu(141)-ZSM-5, Ce(60),Cu(138)-ZSM-5 and the parent Na-ZSM-5 have the same XRD pattern. However, the 500°C-steamed samples show diffraction peak shift to lower 2θ, as shown in Fig. 13b. Hence, the steaming

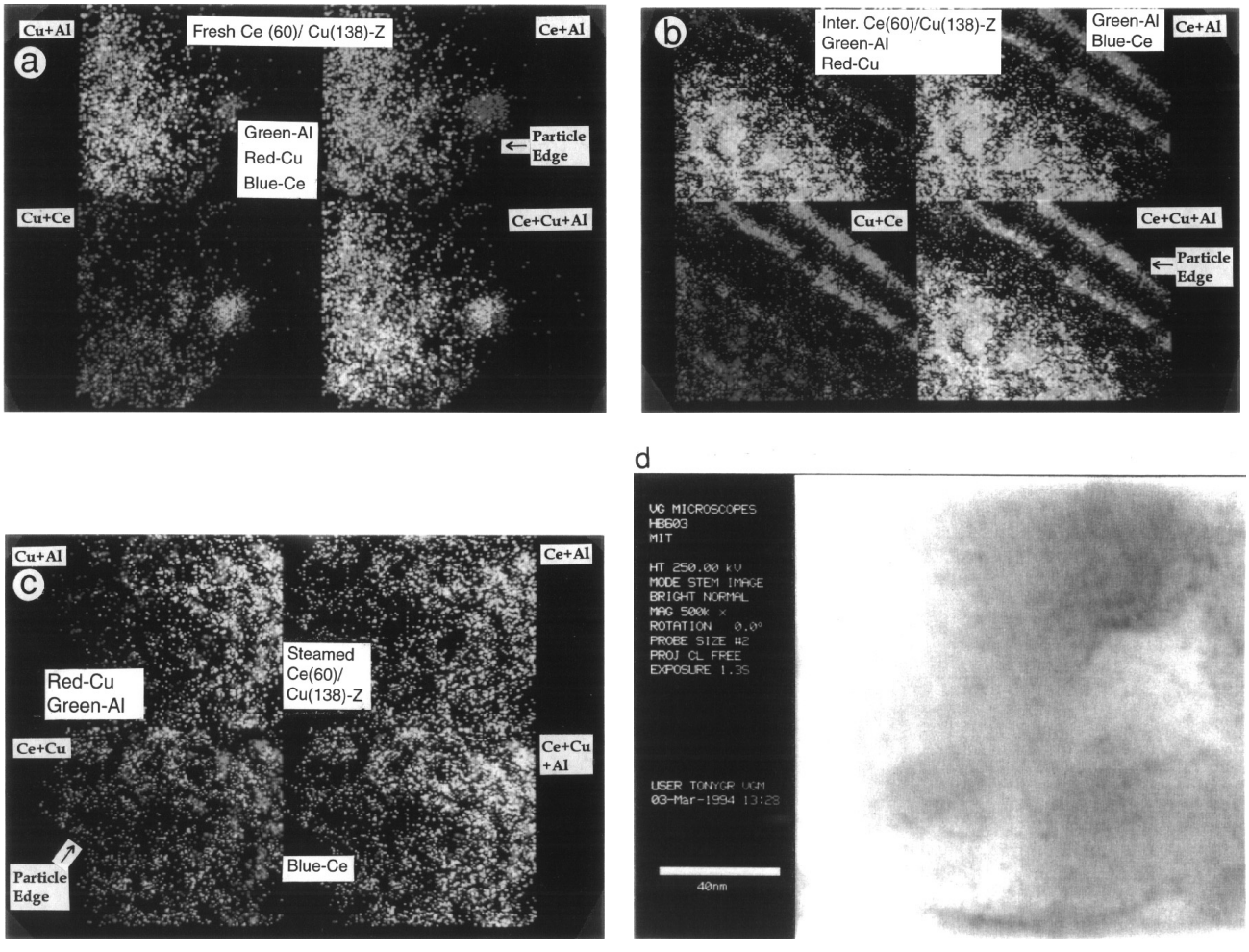

FIG. 10. STEM/X-ray mapping of Al, Cu, and Ce in Ce(60),Cu(138)-ZSM-5. (a) 500°C air-calcined fresh sample; (b) used in 20% H_2O–2% NO–He at 500°C for 10 h; (c) same as (b), then in dry gas (2% NO–He) for 20 h at 500°C (scale of a mapping: 100 nm by 120 nm); (d) STEM picture of (c) showing aggregates (<3 nm).

treatment of samples leads to increased d-spacing of the zeolite crystal, based on Bragg's law. The shift (2θ) for the 500°C-steamed Cu(141)-ZSM-5 sample was higher than that for the 500°C-steamed Ce(60),Cu(138)-ZSM-5, and the 500°C-steamed Na-ZSM-5 material (Fig. 13b and Table 3). The position shifts of the five strongest diffraction peaks and d-spacing of corresponding planes for the parent Na-ZSM-5, 500°C-steamed Na-ZSM-5, fresh and 500°C-steamed Cu(141)-ZSM-5 and Ce(60),Cu(138)-ZSM-5 samples are listed in Table 3.

Compared with the above 500°C-steamed samples, the 400°C-steamed Cu(141)-ZSM-5 and Ce(60),Cu(138)-ZSM-5 (refer to Fig. 6) had smaller diffraction peak shift. It is noteworthy that the 500°C- and 600°C-steamed Na-ZSM-5 materials had similar diffraction peak shifts as did the 500°C- and 600°C-steamed Ce(60),Cu(138)-ZSM-5 catalysts. However, the peak shifts of Na-ZSM-5 were smaller than these of Ce(60),Cu(138)-ZSM-5, as shown in Table 3.

XRD pattern comparisons of the 600°C-steamed Na-ZSM-5 in 20% H_2O–4% O_2–He (14) for 20 h with the 600°C-steamed Ce(60),Cu(138)-ZSM-5 in 20% H_2O–2% NO–He for 10 h are shown in Fig. 14. A "halo" at $2\theta =$ 10–40° indicating amorphous material formation is clearly seen in the former material.

Figure 15 shows the XRD pattern of 500°C-steamed Cu(141)-ZSM-5 in 20% H_2O–He for 10 h. CuO diffraction peaks are observed. However, the CuO peaks were more pronounced in the catalytically-steamed Cu(141)-ZSM-5, Fig. 12.

Cation re-exchange capacity of steamed catalysts. The 500°C- and 600°C-steamed zeolites were also evaluated in terms of their cation uptake capacity after removal of copper with dilute nitric acid according to the procedure described above. Table 2 shows the ICP analyses. The 600°C-steamed Na-ZSM-5 was directly exchanged with copper

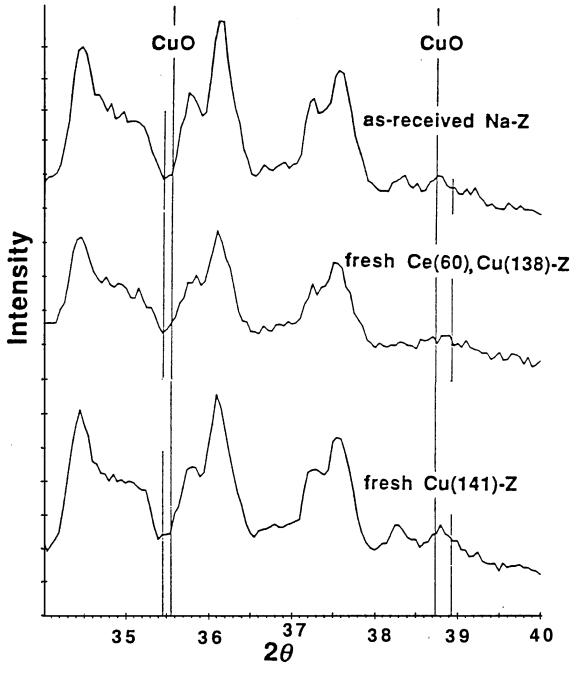

FIG. 11. XRD patterns of fresh, 500°C air-calcined Cu(141)-ZSM-5; fresh, 500°C air-calcined Ce(60),Cu(138)-ZSM-5; and as-received Na-ZSM-5.

acetate solution. Steaming caused a large loss of exchange capacity to this material. After three Cu-ion exchanges under the usual conditions, the measured Al/Cu ratio was only 0.1 compared to 0.7 for the as-received Na-ZSM-5. For the Cu(141)-ZSM-5 samples after wet NO decomposition at 500 and 600°C, the re-exchanged copper ion capacities were Cu/Al = 0.47 and 0.27 respectively. The latter is higher than the Cu/Al value of 0.1 for the 600°C-steamed Na-ZSM-5. The steamed Ce(40),Cu(135)-ZSM-5 samples at 500 and

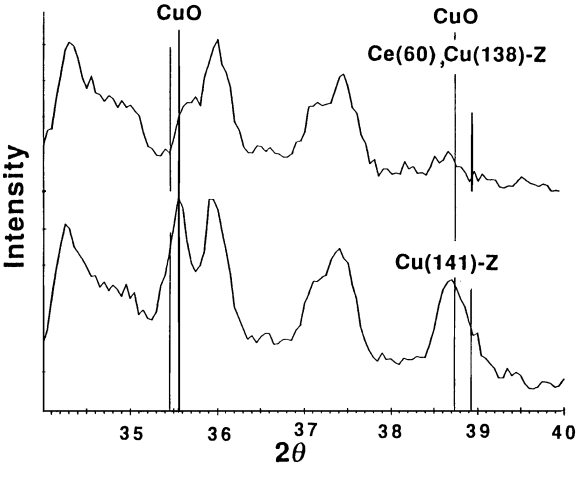

FIG. 12. XRD patterns of catalytically used Cu(141)-ZSM-5; catalytically used Ce(60),Cu(138)-ZSM-5 both after use in 20% H_2O–2% NO–He for 10 h, then in 2% NO–He at 500°C for 20 h.

TABLE 3

Summary of X-Ray Diffraction Peak Shifts

Parent Na-ZSM-5[a]					
2θ (°)	8.05	8.95	23.20	24.00	24.45
d-spacing (Å)	10.9742	9.8726	3.8308	3.7049	3.6378
500°C-steamed Na-ZSM-5[b]					
2θ (°)	7.95	8.85	23.10	23.90	24.40
d-spacing (Å)	11.1120	9.9839	3.8472	3.7202	3.6451
$\frac{\delta d(\text{steamed} - \text{parent})}{d_{\text{fresh}}} \times 100\%$	1.50	1.13	0.43	0.41	0.20
Fresh Cu(141)-ZSM-5 and Ce(60),Cu(138)-ZSM-5					
2θ (°)	8.05	8.95	23.20	24.00	24.45
d-spacing (Å)	10.9742	9.8726	3.8308	3.7049	3.6378
$\frac{\delta d(\text{fresh} - \text{parent})}{d_{\text{parent}}} \times 100\%$	0.00	0.00	0.00	0.00	0.00
500°C-steamed Cu(141)-ZSM-5[b]					
2θ (°)	7.85	8.75	23.05	23.80	24.30
d-spacing (Å)	11.2534	10.0978	3.8554	3.7356	3.6599
$\frac{\delta d(\text{steamed} - \text{fresh})}{d_{\text{fresh}}} \times 100\%$	2.55	2.28	0.64	0.83	0.61
500°C-steamed Ce(60),Cu(138)-ZSM-5[b]					
2θ (°)	7.90	8.80	23.05	23.85	24.35
d-spacing (Å)	11.112	9.9839	3.8308	3.7279	3.6525
$\frac{\delta d(\text{steamed} - \text{fresh})}{d_{\text{fresh}}} \times 100\%$	1.50	1.13	0.64	0.62	0.40

[a] As-received.

[b] At 500°C in He for 2 h, then in 2% NO–He for 4 h, then in 20% H_2O–2% NO–He for 10 h followed by 2% NO–He for 20 h.

600°C showed higher copper re-exchange capacities with Cu/Al values of 0.60 and 0.35, respectively. This Ce,Cu-ZSM-5 material was used in place of Ce(60),Cu(138)-ZSM-5 for the comparisons shown in Table 2.

In a separate control experiment, Ce(60)-ZSM-5 was treated under a similar wet NO decomposition condition at 600°C. The steamed sample had medium-high copper ion exchange capacity with Cu/Al = 0.41 (Table 2). This shows that the steamed cerium ion-exchanged ZSM-5 retained more copper ion exchange sites than the 600°C-steamed Na-ZSM-5.

Catalytic activities of the copper re-exchanged ZSM-5 materials prepared from the steamed catalysts as well as the Cu-ZSM-5 synthesized from the 600°C-steamed Ce(60)-ZSM-5 were evaluated in 2% NO–He at 500°C and W/F = 1.0 g s/cm^3. However, it was found that not all re-exchanged copper ions were active for NO decomposition. Table 4 shows comparisons of the NO conversions over the Cu re-exchanged materials with those over the respective steamed catalysts, and fresh Cu-ZSM-5 prepared directly from the as-received Na-ZSM-5.

The residual catalytic activity of the Cu(141)-ZSM-5 after 500°C-steaming was the same as that of the Cu(94)-ZSM-5 resulted from re-exchanging the 500°C-steamed Cu(141)-ZSM-5 sample (Table 4). However, the Cu re-exchanged

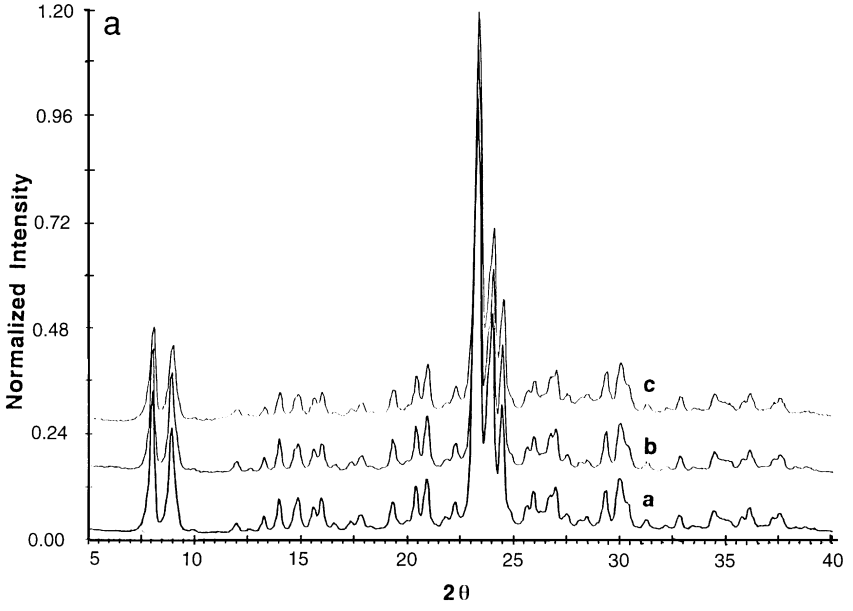

FIG. 13a. (a) As-received Na-ZSM-5; (b) fresh 500°C air-calcined Cu(141)-ZSM-5; (c) fresh 500°C air-calcined Ce(60),Cu(138)-ZSM-5.

catalyst prepared from the 500°C-steamed Ce(40),Cu(135)-ZSM-5 showed lower conversion of NO to N_2 (30.1%) than the original steamed material (58%). Also shown in Table 4 are conversions of NO to N_2 over fresh Cu-ZSM-5 materials containing the same nominal Cu/Al ratios. These materials have much higher catalytic activity than the Cu re-exchanged ZSM-5 materials.

Dynamic change of copper in Cu-ZSM-5 and Ce,Cu-ZSM-5. The surface ratios of copper, cerium, and oxygen to silicon of fresh and used Cu(141)-ZSM-5 and Ce(60),Cu(138)-ZSM-5 samples were measured by XPS. Atomic ratios of cerium, and oxygen to silicon are shown in Table 5, while Fig. 16 shows the Cu/Si ratios for the Cu(141)-ZSM-5 and Ce(60),Cu(138)-ZSM-5 catalysts after various

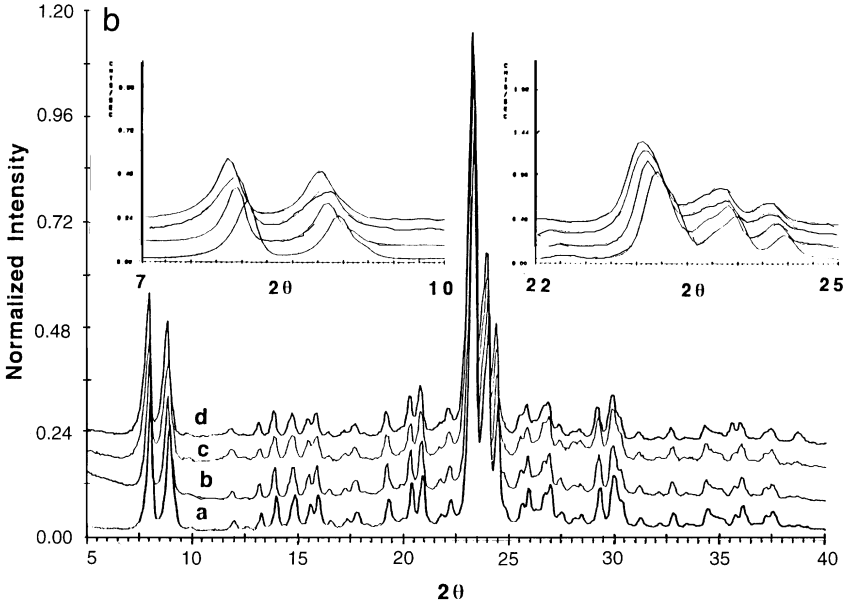

FIG. 13b. (a) As received Na-ZSM-5; (b) 500°C-steamed Na-ZSM-5 in 20% H_2O–4% O_2–He; (c) 500°C-steamed Ce(60),Cu(138)-ZSM-5; (d) the 500°C-steamed Cu(141)-ZSM-5 in 20% H_2O–2% NO–He for 10 h, then in 2% NO–He for 20 h. Insets: $2\theta = 7$–$10°$ (upper left); $2\theta = 22$–$25°$ (upper right).

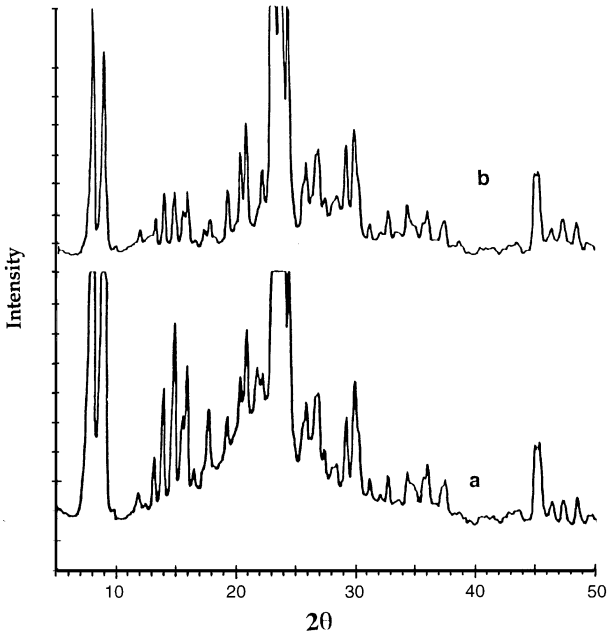

FIG. 14. XRD patterns of (a) 600°C-steamed Na-ZSM-5 (20 h) in 20% H_2O–4% O_2–He (14) and (b) 600°C-steamed Ce(60),Cu(138)-ZSM-5 (10 h) in 20% H_2O–2% NO–He.

treatments. The bulk Cu/Si ratio measured by ICP is equal to 0.035 for both the Cu(141)-ZSM-5 and Ce(60),Cu(138)-ZSM-5, while the bulk Ce/Si is equal to 0.01 in the latter. The O/Si of the as-received Na-ZSM-5 equals 2.72. The O/Si ratios of the as-synthesized, treated-1, -2, and -3 samples for the two catalysts are approximately constant, and a little higher than the value of 2.72, especially for Ce,Cu-ZSM-5 (see Table 5).

Figure 16 shows the change of Cu/Si ratio with treatment for the Ce(60),Cu(138)-ZSM-5. The Cu/Si ratio (= 0.395) of the as-synthesized (uncalcined) sample is much higher than bulk concentration (Cu/Si = 0.035). After treatment-1, copper migrates into the zeolite leading to lower Cu/Si

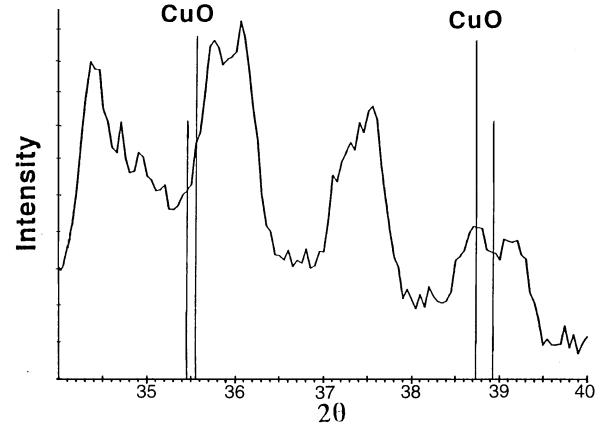

FIG. 15. XRD analysis of Cu(141)-ZSM-5 steamed in 20% H_2O–He at 500°C for 10 h.

TABLE 4

Activity Comparisons of Fresh, Steamed and Copper Re-exchanged ZSM-5

Catalysts	NO Conversion to N_2 (%)[a]
Cu re-exchanged Cu(94)-ZSM-5 from 500°C-steamed Cu(141)-ZSM-5[b]	28.0
Cu re-exchanged Cu(120)-ZSM-5 from 500°C-steamed Ce(40)/Cu(135)-ZSM-5[2]	30.1
Cu exchanged Cu(108)-ZSM-5 from 600°C-steamed Ce(60)-ZSM-3[b]	13.7
Cu(141)-ZSM-5 after 500°C-steaming	29.0
Ce(40),Cu(135)-ZSM-5 after 500°C-steaming	58.0
Cu exchanged Cu(20)-ZSM-5 from 600°C-steamed Na-ZSM-5	5.0
Fresh Cu(20)-ZSM-5[c]	7.0
Fresh Cu(82)-ZSM-5[c]	65.0
Fresh Cu(94)-ZSM-5[c]	72.0
Fresh Cu(120)-ZSM-5[c]	82.5
Fresh Cu(141)-ZSM-5	92.0

[a] In 2% NO–He at 500°C and W/F = 1.0 g s/cm^3 (NTP).
[b] Copper re-exchange according to the procedure of Table 2.
[c] Data are from Fig. 3.6 in (20).

value, from 0.395 to 0.071. When water vapor was present in the reactant stream, i.e., under treatment-2, copper migrated out and enriched the surface region of the catalyst particles. The same amount of surface copper moved back to the bulk of the catalyst again under treatment-3, which indicates copper redistribution. These results are in good agreement with the STEM/EDX analyses of Figs. 10b and 10c, and with the XRD data of Fig. 12.

TABLE 5

O/Si and Ce/Si Ratios in Cu(141)-, and Ce(60),Cu(138)-ZSM-5[a]

	Treatment[b]							
	As-synthesized		1		2		3	
Catalyst	O/Si	Ce/Si	O/Si	Ce/Si	O/Si	Ce/Si	O/Si	Ce/Si
Cu(141)-ZSM-5[c]	2.80		2.78		2.71		2.74	
Ce(60),Cu(138)-ZSM-5[c,d]	3.48	0.27	3.35	0.28	3.44	0.24	3.20	0.23
Ce(11),Cu(119)-ZSM-5[e]		0.002						
Parent Na-ZSM-5	2.72							

[a] Atomic ratios were measured by XPS with Mg$K\alpha$.
[b] Treatments: (1) in He for 2 h, then in 2% NO–He at 500°C for 4 h, (2) in 20% H_2O–2% NO–He at 500°C for 10 h following treatment-1; (3) in 2% NO–He at 500°C for 20 h following treatment-2.
[c] Bulk value of Cu/Si = 0.035, measured by ICP.
[d] Bulk value of Ce/Si = 0.01, measured by ICP.
[e] Bulk value of Ce/Si = 0.002, measured by ICP.

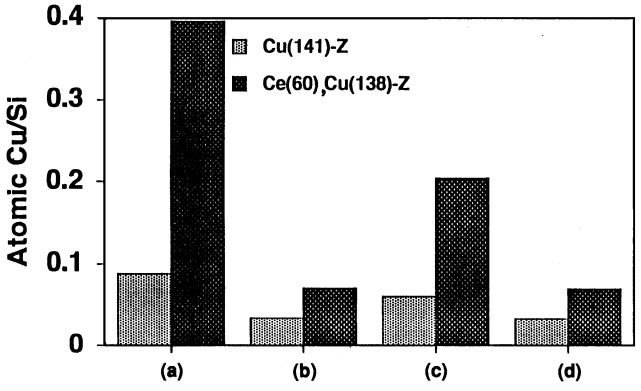

FIG. 16. XPS-measured surface Cu/Si ratios of Ce(60),Cu(138)-ZSM-5, and Cu(141)-ZSM-5 catalysts after various treatments: (a) fresh and uncalcined; (b) in 2% NO–He for 4 h at 500°C; (c) then in 20% H_2O–2% NO–He at 500°C for 10 h; (d) then in 2% NO–He at 500°C for 20 h.

Cerium ions were not as mobile as copper ions. This is indicated by Ce concentrations on the surface regions of the Ce(60),Cu(138)-ZSM-5 materials only slightly different under treatments-2 and -3, than for the as-synthesized sample (see Table 5). The surface cerium concentration remained much higher than the bulk value. However, the Ce/Si ratio on the surface of the Ce(11),Cu(119)-ZSM-5 material was equal to the bulk value.

Surface Cu/Si ratios in Cu(141)-ZSM-5 were lower than in Ce(60),Cu(138)-ZSM-5 under the same treatments, as shown in Fig. 16. The as synthesized (uncalcined) sample had higher copper concentration (Cu/Si = 0.088) than the bulk (0.035). After treatment-1, copper migrated into the zeolite leading to surface Cu/Si equal to the bulk value. The Cu/Si increased to 0.06 after treatment-2, and decreased again to the bulk value after water vapor was removed from the reaction stream (treatment-3). Thus, the CuO particles seen in Figs. 9b and 12 do not appear to form on the zeolite surface.

DISCUSSION

Ce,Cu-ZSM catalyst preparation. The preparation of Ce-ZSM-5 by ion exchange at 85°C, 2h achieves partial exchange with Na ions, as shown in Table 1. In addition, during the exchange, partial protonation of the sites must have occurred as indicated by the lack of charge balance in Table 1. The data of Table 1 also show that a limit to cerium ion exchange exists after two sequential exchanges. Thus, the higher uptake of Ce in the third exchange must be due to surface deposition rather than ion exchange. STEM/EDX and XPS data confirm this (Fig. 10 and Table 5). However, the oxidic cerium is not highly crystallized, as no CeO_2 peaks could be detected by XRD. Based also on the luminescence evidence of Ce^{3+} in both low- and high-cerium containing ZSM-5 samples (Ce^{3+} luminescence signal intensity does not increase linearly with Ce loading [20]); XPS evidence (the surface Ce/Si is equal to the bulk value for Ce(11),Cu(119)-ZSM-5; but much higher than the bulk value for the Ce(60),Cu(138)-ZSM-5); and STEM/EDX evidence (uniform bulk signal of cerium), we conclude that our working catalysts comprise a small fraction of cerium as Ce^{3+} ions associated with the framework aluminum as well as Ce^{4+} in oxidic form on the zeolite surface; the latter is predominant in the Ce(60)-ZSM-5 and Ce(60),Cu(138)-ZSM-5, while the former dominates in the Ce(11)-ZSM-5 and Ce(11),Cu(119)-ZSM-5 materials. The ion-exchanged Ce^{3+} species in ZSM-5 are probably complex hydroxy-ions with one or two positive charges. Isolated Ce^{3+} ions are highly unlikely in view of the sparse Al distribution in the ZSM-5.

It appears that the ion-exchanged Ce^{3+} species promote the catalyst activity, as indicated by activity comparisons of Ce(60),Cu(138)-ZSM-5 and impregnated Ce(60)/Cu(136)-ZSM-5. The latter catalyst contains Ce^{4+} largely on the surface. This is because there is little possibility for ion exchange between the Cu(136)-ZSM-5 and cerium ions under the conditions used for impregnation (Table 1). In Fig. 1, the concerted effect of Ce^{3+} and active copper sites is clearly shown by higher NO conversion to N_2 over the Ce(11),Cu(119)-ZSM-5 than the Cu(141)-ZSM-5 catalyst in the low temperature range (300–450°C). The reduced effectiveness of Ce(60),Cu(138)-ZSM-5 in this region may be due to lower Ce^{3+} species concentration (20). In catalysts prepared by sequential exchange, the Ce^{3+} ion was exchanged first; then air calcination was used prior to exchanging the copper ions. The role of heat treatment on the cerium stability in ZSM-5 may be similar to that of Ce–Y zeolite, which has been reported to cause stronger binding of Ce cations to the zeolite framework in Na-Y (21). It is interesting that even after several such air calcinations, a small fraction of Ce^{3+} exists in the zeolite, as shown in Fig. 8.

Steaming effects. Structural changes of zeolites due to high temperature steaming are well established in the literature (22). While the highly siliceous ZSM-5 structure is more hydrothermally stable than the Y-zeolite, severe steaming at 600°C can lead to extensive structural changes (14). We have found that steaming of Na-ZSM-5 at 500°C does not change the XRD pattern, except for a small diffraction peak shift, and also retains the micropore volume and the Cu^{2+} uptake capacity of the fresh material (14). The H-ZSM-5 form is the most hydrothermally unstable, while M-ZSM-5, where M is alkali or alkaline earth metals, has been reported as more stable (23, 24). Using ^{27}Al-NMR, Grinsted *et al.* (25) have reported aluminum stabilization in H-ZSM-5 by Cu cations after the sample had been steamed at 700°C. The results of the previous section and Fig. 14 show that Ce,Cu-ZSM-5 is more stable structurally than the Na-ZSM-5 material after exposure to 20% H_2O-containing

gas at 600°C for 10 h. The appearance of an amorphous background (halo) at $2\theta = 10$–40° is clearly seen for the Na-ZSM-5 material but not for the Ce,Cu-ZSM-5 in Fig. 15. The NO conversion to N_2 over Ce(60),Cu(108)-ZSM-5, where the copper was exchanged after 600°C-steaming of the Ce(60)-ZSM-5 material, was 13.7% (see Table 4), while the Cu(20)-ZSM-5 prepared from the 600°C-steamed Na-ZSM-5 showed only 5% conversion of NO to N_2.

Hydrated and hydrolyzed copper complexes may be formed when Cu-ZSM-5 is exposed to water vapor at reaction temperatures. These copper complexes are more mobile than bare Cu^{2+} cations due to lower surface charge density. Therefore, hydrolyzed copper complexes migrate in the zeolite cavities, which leads to protonation (Brønsted acidity) of the sites left behind. Upon dehydration, aggregation can lead to CuO particle formation and catalyst deactivation. The following simplified scheme is proposed:

$$Cu^{2+} = Z(\text{active isolated } Cu^{2+}) + x\ H_2O \leftrightarrow Cu^{2+}(H_2O)_x = Z \quad [1]$$

The electrostatic field of divalent Cu cations is assumed to generate protons according to the equilibrium reactions (26, 27)

$$Cu^{2+}(H_2O)_x = Z \leftrightarrow [Cu^{2+}(OH)^-(H_2O)_{x-1}]^+\text{-}Z\text{-}H^+ \quad [2]$$

and

$$[Cu^{2+}(OH)^-(H_2O)_{x-1}]^+\text{-}Z\text{-}H^+ \leftrightarrow Cu(OH)_2 + H^+\text{-}Z\text{-}H^+ + (x-2)H_2O \quad [3]$$

Finally, CuO is formed by the decomposition reaction

$$Cu(OH)_2 \leftrightarrow CuO + H_2O, \quad [4]$$

where Z is the ZSM-5 substrate, $Cu^{2+}(H_2O)_x$ and $[Cu(OH)]^+$ are representative of hydrated and hydrolyzed copper complexes, and H^+ is a Brønsted acid. In wet-NO decomposition tests, the values of the steady state catalytic activities at different water vapor contents suggest that an equilibrium is established between Cu^{2+} and water vapor; otherwise 2% H_2O in the reaction stream is enough to deactivate all the active copper sites. This is because the total number of H_2O molecules fed through the catalyst bed during the 10 h steaming was about 100 times as high as the Cu atoms in Cu(141)-ZSM-5 or Ce(60),Cu(138)-ZSM-5.

The proposed mechanism of Cu-ZSM-5 deactivation is supported by the appearance of CuO diffraction peaks on the XRD pattern of Cu(141)-ZSM-5 after the material was steamed in 20% H_2O–He at 500°C for 10 h, i.e., in the absence of reaction and oxygen. Figure 15 shows this result. By comparing the XRD patterns of Cu(141)-ZSM-5 in Fig. 15 (no reaction) and 12 (wet NO decomposition) we see that CuO formation is more extensive for the latter. Presently, we do not have an explanation for this apparent reaction-enhanced agglomeration/sintering of CuO.

Reaction-induced structural changes. The cyclic dry/wet NO decomposition tests over Cu(141)-ZSM-5 and Ce(60),Cu(138)-ZSM-5, Figs. 4–7, clearly show that both reversible and irreversible loss of active copper sites take place under the conditions employed. Moreover, a beneficial effect of the presence of cerium is displayed by higher wet-gas activity as well as higher dry-gas activity recovery. In all cycles, a rather rapid (~2 h) approach to steady-state conversion of NO to N_2, indicates an equilibrium process at play. This can be thought of as a hydration–dehydration process and is, thus, a function of water content and temperature. Irreversible loss of activity may occur either through zeolitic structural changes due to steaming or copper migration/aggregation or both. We discuss below the plausible pathways for the observed activity loss on the basis of the data collected in this work.

The data of Fig. 3 show that the excessively exchanged Cu-ZSM-5 recovered 33% of its initial dry-gas activity, while Cu(72)-ZSM-5 permanently lost its activity. The effect of cerium presence is significant for the ion-exchanged Ce-ZSM-5, e.g., Ce(11),Cu(119)-ZSM-5, but negligible for the cerium impregnated, excessively copper ion exchanged Ce(60)/(136)-ZSM-5 material. Hence, the presence of Ce^{3+} species is beneficial. In regards to copper ions, these results indicate that two coordinations exist: one stable and one unstable in the presence of water.

The characterization results shown in Figs. 9–13 and 16 may be used to show that CuO particle formation (sintering) causes the observed irreversible loss of activity after wet-gas NO decomposition. Cerium suppresses this sintering as indicated by the absence of CuO phase from the steamed Ce(60),Cu(138)-ZSM-5 in Figs. 12 and 10. In this material, cerium exists primarily as an oxidic phase on the surface, as seen in Fig. 10a and Table 5, along with a certain amount of Ce^{3+} ions in the zeolite channels, as shown in Figs. 10a and 8 and Table 1. From Figs. 10 and 16, it can be concluded that Cu cations are not only associated with framework aluminum but also with cerium ions. Yet, copper ion species remain mobile under various conditions as Fig. 16 clearly shows. Copper ion migration into ZSM-5 has been reported by Shpiro *et al.* (28) after heat treatment of the fresh Cu-ZSM-5 in oxygen, and nitric oxide. However, Haack *et al.* (29) found that copper migrated out to the crystal surface region after heat treatment at 500°C in oxygen and argon following severe reduction in hydrogen. In Cu–Y zeolite, copper has much less mobility (30) than in Ce, Cu-ZSM-5.

Certainly, cerium does not seem to suppress the mobility of Cu ions, e.g., Figs. 10b, 10c, and 16. However, it enhances the dispersion of copper, and thus, its reversibility. It has been reported that copper in cerium oxide exists as small clusters of Cu^{1+} state in highly dispersed form (31).

Figure 9b and the corresponding XRD pattern shown in Fig. 12 show Cu aggregation and CuO particle formation. The XPS analysis, however, in Fig. 16, does not show accumulation of Cu on the surface. Rather, a reversible migration to the surface (upon steaming) and back into the channels (after removal of H_2O) is observed. Thus, the irreversible CuO particle formation must occur inside the zeolite channels! The size of these CuO particles is too large to be accommodated by mere crystal expansion. We can only conclude that the zeolite structure is damaged around these CuO particles. Crystal expansion is also indicated by the increase of d-spacing for the 500°C-steamed materials, which changes in the following order: Cu(141)-ZSM-5 > Ce(60),Cu(138)-ZSM-5 > Na-ZSM-5. This order is the same as the CuO particle sizes found in the above materials. However, the damage remains sparse for the total loading of copper (∼3 wt.%) used here. Consequently, the XRD pattern does not change significantly.

Figure 14 shows amorphous material formation for the 600°C-steamed Na-ZSM-5, but not for the 600°C-steamed Ce(60),Cu(138)-ZSM-5. However, the diffraction peak shift on the XRD of the former material was less than for the latter. The results from XRD, XPS, and STEM/EDX characterization provide strong evidence that the more pronounced diffraction peak shifts in the steamed Cu-containing materials were caused by CuO particle formation inside the zeolite channels.

Upon water vapor removal from the reactant stream, only a part of the dry gas-catalytic activity is restored. This partial activity recovery must be mainly attributed to dehydration of the hydrolyzed or hydrated copper complexes. Any CuO particles formed during the process of wet NO-decomposition, however, represent irreversible loss of activity. In recent work, Kharas *et al*. (17) showed that such sintering is fast and extensive even in short-time runs at 600 and 800°C in 10% H_2O-containing lean-engine exhaust gases. The corresponding structural changes of the zeolitic matrix were reported to be minor, even though XRD analysis indicated amorphous material formation gradually with temperature over the range of $2\theta = 10$–40°. In the long-time hydrothermal tests reported here, structural changes (e.g., diffraction peak shifts) do occur, even at lower temperatures. However, we attribute those to de-stabilization of the zeolite structure upon migration of copper ion complexes away from the framework aluminum. Thus, according to the scheme of reactions (2) and (3), a partially protonated ZSM-5 is formed, which is less stable than the metal exchanged form, i.e., more prone to dealumination by steaming. As Figs. 4–7 and Tables 2 and 4 indicate, this phenomenon is more pronounced at the higher temperatures of 500 and 600°C. At 400°C and low water vapor content, crystalline CuO is not formed even after several days in operation, and this preserves the structural integrity of the zeolite as well. It is plausible that aggregation/sintering of CuO particles is very slow at the lower temperature of 400°C. Instead, fine copper oxide clusters may form, which can exchange back with the zeolite protons upon removal of the water (see Fig. 6 data for Cu(141)-ZSM-5). The formation of $[Cu–O–Cu]^{2+}$ clusters in Cu-ZSM-5 has been proposed in the recent literature (32, 33).

It is noteworthy that the presence of Ce^{3+} is beneficial even at the mild conditions of Fig. 6. The possible explanations for the positive effect of cerium ions on the hydrothermal stability of Cu-ZSM-5 are: (i) cerium imparts stabilization of copper ions in the active coordination with the Al–O of the framework. This would suppress copper ion complex migration away from the framework aluminum followed by dealumination of the resulting protonated AlO_2^- site; (ii) even when migration occurs, the cerium–copper interaction is strong and prevents aggregates from forming crystallites of CuO that may sinter and be lost irreversibly. Rather, highly dispersed copper clusters may prevail and these can slowly recover activity by exchanging with protons on AlO_2^- sites (see Fig. 6). Hydration of the cerium ions may also occur, but this can not be used to explain the consistently twice as high activity of Ce(60),Cu(138)-ZSM-5 over the Cu(141)-ZSM-5 material at 500°C and all wet gas compositions (2–20% H_2O, see Figs. 4 and 5).

Finally, the results with re-exchanged materials after steaming and extraction of the ionic copper are interesting as they both complement the XRD and STEM/EDX analyses as well as provide some new information. As Table 2 shows, the high copper re-exchange capacity of the steamed materials does not correlate with the resulting low activity for NO decomposition (Table 4). This indicates that the steamed materials contain either extra-framework tetrahedral aluminum or other negatively charged sites, e.g., hydroxylated fragments (34) that have copper uptake capacity but no activity. In the re-exchanged materials copper deposition on the surface can be ruled out since the color of the re-exchanged materials remained light blue and no CuO phase was detected by XRD. Also, the process of copper extraction used here prior to re-exchange does not extract framework aluminum. This is shown in Table 2. The fresh parent Na-ZSM-5 zeolite, after the same treatment (washed with 0.05M HNO_3 solution at room temperature for 4 h), had identical copper exchange capacity to the untreated material, and the copper was equally active in both cases. It has been reported that even with 1*M* HNO_3 solution, i.e., much higher concentration than the 0.05*M* solution used here, only non-framework aluminum is partially extracted from steamed ZSM-5 (35). The Cu re-exchanged catalyst prepared from the 500°C-steamed Ce(40),Cu(135)-ZSM-5 according to the above technique was less active for NO decomposition than the original steamed material (Table 4). This suggests the existence of a stabilized Cu-. . . Ce-. . . Al–O site, which is active for NO decomposition, but is destroyed in dilute HNO_3 solution.

These metastable active sites exist only in the presence of Ce ions in Cu-ZSM-5, and serve to prove that cerium enhances the stability of active copper sites in wet NO decomposition.

CONCLUSION

We have shown that cerium addition to Cu-ZSM-5 promotes the activity of the latter for the NO decomposition in wet gas streams at temperatures in the range of 400–600°C. From extensive analysis of unmodified Cu-ZSM-5, it appears that the mechanism of copper deactivation in wet NO decomposition is twofold: (i) equilibrium hydration (reversible); (ii) copper ion species migration/aggregation and CuO crystallite formation/sintering (irreversible). The second path is thermally activated, hence, high temperature of reaction will exacerbate it. We think that dealumination happens as a result of partial protonation of sites vacated by the mobile copper ion complexes; thus, dealumination appears to be a secondary path in the deactivation process. The partial recovery of dry-gas activity upon removal of water indicates that not all copper sites are equally unstable in wet gas streams; there is a fraction of active copper sites of apparently strong coordination with the framework (nonmobile). Cerium serves to stabilize additional copper sites.

Certainly, the Ce,Cu-ZSM-5 material used in this work is not optimized. If the presence of Ce^{3+} ions is important, the Ce(60),Cu(138)-ZSM-5 contains only a small fraction of these. Additional work on catalyst preparation is needed. Overall, emphasis should be placed on promoting the low-temperature ($\leq$450°C) activity of Cu-ZSM-5, because at low temperatures both dealumination and thermal sintering of CuO crystallites will be suppressed. Promoters, such as cerium, which provide hydrothermal stability need to be further studied since they also provide low-temperature activity enhancement.

ACKNOWLEDGMENTS

The guidance by Professor A. F. Sarofim of the MIT Department of Chemical Engineering is greatly appreciated by Y. Zhang. The discussion of the XRD analysis with Professor B. J. Wuensch of the MIT Department of Materials Science and Engineering is also appreciated. Dr. A. Garratt-Reed of the MIT Center of Materials Science and Engineering is acknowledged for his assistance with the STEM/EDX analyses, and Professor S. L. Suib of the Department of Chemistry at the University of Connecticut is acknowledged for his assistance with the luminescence analyses. We also thank the reviewers of this paper. This research has been financially supported by the U.S. Department of Energy (Grant DE-FG22-91PC923), the Gas Research Institute (Grant 5093-260-2580), and the Italian Power Authority, ENEL-CRAM, of Milan.

REFERENCES

1. Iwamoto, M., Furukawa, H., Mine, Y., Uemura, F., Mikuriya, S., and Kagawa, S., *J. Chem. Soc., Chem. Commu.* **15**, 1272 (1986).
2. Iwamoto, M., Misono, M., Moroka, Y., and Kimura, S., *in* "Future Opportunities in Catalytic and Separation Technology, Studies Surface and Catalysis," p. 121, Elsevier, Amsterdam, 1990.
3. Li, Y., and Hall, W. J., *J. Catal.* **129**, 202 (1991).
4. Li, Y., and Armor, J., *Appl. Catal.* **76**, L1 (1991).
5. Shelef, M., *Catal. Lett.* **15**, 305–310 (1992).
6. Zhang, Y., Leo, K., Sarofim, A. F., Hu, Z., and Flytzani-Stephanopoulos, M., *Catal. Lett.* **31**, 75–89 (1995).
7. Lei, G. D., Adelman, B. J., Sárkány, J., and Sachtler, *Appl. Catal. B: Environ.* **5**, 245–256 (1995).
8. Matsuoka, M., Matsuda, E., Tsuji, K., Yamashita, and Anpo, M., *Chem. Lett.*, 375 (1995).
9. Lee, C.-Y., Choi, K.-Y, and Ha, B.-H., *Appl. Catal. B: Environ.* **5**, 7–21 (1995).
10. Kucherov, A. V., Gerlock, J. L., and Shelef, M., *J. Catal.* **152**, 63–69 (1995).
11. Kucherov, A. V., Gerlock, J. L., Jen, H. W., and Shelef, M., *Zeolites* **15**, 9–14 (1995).
12. Kagawa, S., Ogawa, H., Furukawa, H., and Teraoka, Y., *Chem. Lett.*, 407 (1991).
13. Zhang, Y., and Flytzani-Stephanopoulos, M., *in* "Environmental Catalysis" (J. Armor, Ed.), p. 7, ACS Symposium Series, Vol. 552, ACS, Washington, DC, 1994.
14. Zhang, Y., Sun, T., Sarofim, A. F., and Flytzani-Stephanopoulos, M., *in* "Reduction of Nitrogen Oxide Emissions," (U. S. Ozkan, Ed.), Chap. 9, p. 133, ACS Symposium Series, Vol. 587, ACS, Washington, DC, 1995; also in *ACS Preprints* **39**, 171 (1994).
15. Iwamoto, M., Yohiro, H., Tanda, K., Mizuno, N., Mine, Y., and Kagawa, S., *J. Phys. Chem.* **95**, 3727 (1991).
16. Li, Y., and Hall, W. K., *J. Phys. Chem.* **94**, 6148 (1990).
17. Kharas, K. C. C., Robota, H. J., and Datye, A., *in* "Environmental Catalysis" (J. Armor, Ed.), p. 39, ACS Symposium Series Vol. 552, ACS, Washington, DC, 1994.
18. Tanguay, J. F., and Suib, S. L., *Catal. Rev.-Sci. Eng.* **29**, 1 (1987).
19. Bennett, J. M., and Smith, J. V., *Mater. Res. Bull.* **4**, 343 (1969).
20. Zhang, Y., Sc.D. Thesis, Department of Chemical Engineering, Massachusetts Institute of Technology, 1995.
21. Moscou, L., and Lakeman, M. J., *J. Catal.* **16**, 173 (1970).
22. Lago, R. M., Haag, W. O., Mikovsky, R. J., Olson, D. H., Hellring, S. H., Schmidt, K. D., and Kerr, G. T., *in* "Proceedings of the 7th International Zeolite Conference," p. 667, Tokyo, 1986.
23. Suzuki, K., Sano, T., Shoji, H., Murakami, T., Ikai, S., Shin, S., Hagiwara, H., and Takaya, H., *Chem. Lett.*, 1507 (1987).
24. Fujisawa, K., Sano, T., Suzuki, K., Okado, H., Kawamura, K., Kohtoku, Y., Shin, S., Hagiwara, H., and Takaya, H., *Chem. Soc. Japan* **60**, 791 (1987).
25. Grinsted, R. A., Jen, H. W., Montreuil, C. N., Rokosz, M. J., and Shelef, M., *Zeolites* **13**, 602 (1993).
26. Uytterhoeven, J. B., Schonheydt, R., Liengme, B. V., and Hall, W. K., *J. Catal.* **13**, 425 (1969).
27. Jacobs, P. A., *in* "Carboniogenic Activity of Zeolites," p. 45, Elsevier, Amsterdam, 1977.
28. Shpiro, E. S., Grüner, W., Joyner, R. W., and Baeva, G. N., *Catal. Lett.* **24**, 159 (1994).
29. Haack, L. P., and Shelef, M., *in* ACS Symposium Series, Vol. 552, p. 66, Washington, DC, 1994.
30. Suib, S. L., Stucky, G. D., and Blattner, R. J., *J. Catal.* **65**, 179 (1980).
31. Liu, W., and Flytzani-Stephanopoulos, M., *J. Catal.* **153**, 304, 317 (1995).
32. Sárkány, J., d'Itri, J. L., and Sachtler, W. M. H., *Catal. Lett.* **16**, 241 (1992).
33. Sárkány, J., and Sachtler, W. M. H., *in* "Catalysis by Microporous Materials," p 649, Studies in Surface Science and Catalysis, Vol. 94, 1995.
34. Loeffler, E., Lohse, U., Peuker, Ch., Oehlmann, G., Kustov, L. M., Zholobenko, V. L., and Kazansky, V. B., *Zeolites*, 10 (April/May 1990).
35. Loeffler, E., Peuker, Ch., and Jerschkewitz, H.-G., *Catal. Today* **3**, 415 (1988).